Research Square

Preprints are preliminary reports that have not undergone peer review. They should not be considered conclusive, used to inform clinical practice, or referenced by the media as validated information.

American orographic control of simulated Pacific rainfall and warming patterns

Xi Chen

xi_chen5@brown.edu

Brown University https://orcid.org/0009-0007-9542-6141

Jung-Eun Lee

Department of Geological Sciences, Brown University

Article

Keywords:

Posted Date: October 20th, 2026

DOI: https://doi.org/10.21203/rs.3.rs-9569771/v1

License: This work is licensed under a Creative Commons Attribution 4.0 International License. Read Full License

Additional Declarations: There is **NO** Competing Interest.

American orographic control of simulated Pacific rainfall and warming patterns

Xi Chen[1,*] and Jung-Eun Lee[1]

[1]Department of Earth, Environmental and Planetary Sciences, Brown University, Providence, 02912, RI, USA.

*Corresponding author: Xi Chen, xi_chen5@brown.edu

Abstract

Pacific sea-surface warming patterns influence regional rainfall and the pace of global warming by shaping atmospheric circulation and cloud feedbacks, but climate models still struggle to reproduce Pacific rainfall biases and recent warming patterns. Here we show that one source of these errors is the smoothed representation of the Rockies, Central American cordillera and Andes in coarse-resolution climate models. In experiments that restore more realistic peak elevations, higher American mountains reduce excessive moisture transport from the Atlantic and Amazon regions into the Pacific, weaken the spurious southern tropical rain band and reduce Pacific sea-surface temperature biases. In historical simulations, the same topographic change produces a more realistic recent Pacific warming pattern, especially over the northeastern Pacific, by increasing low-cloud radiative cooling. These results identify smoothed American orography as a physically interpretable and potentially correctable model error with implications for Pacific rainfall, warming-pattern biases, regional climate projections and regional climate risk.

Introduction

The Pacific Ocean exerts an outsized influence on global and regional climate by organizing tropical rainfall, atmospheric circulation, marine clouds, and radiative feedbacks[1,2]. These climatic effects depend strongly on the spatial pattern of Pacific sea-surface temperature change, which shapes regional hydroclimate projections and estimates of climate sensitivity. Observations during 1979–2013 show enhanced warming in the western tropical Pacific, muted warming or cooling in parts of the eastern equatorial Pacific, and cooling over portions of the Southern Ocean, producing a La Niña-like trend pattern[2–4]. This pattern has been linked to the recent slowdown in global-mean surface warming[5] and affects energy-budget estimates of equilibrium climate sensitivity and transient climate response[6–8]. Yet successive generations of coupled climate models, including CMIP5 and CMIP6, generally fail to reproduce the observed pattern, instead simulating excessive warming in the eastern Pacific and Southern Ocean or a more El Niño-like tropical Pacific response[3,4,8].

Why models miss this pattern remains unresolved. Previous studies have identified several mechanisms that can favor La Niña-like Pacific SST trends. Some emphasize changes in atmospheric and oceanic circulation: strengthened Pacific trade winds can cool the central-to-eastern tropical Pacific and increase subsurface ocean heat uptake, while Southern Ocean cooling can influence tropical and subtropical Pacific SSTs through atmospheric and coupled feedbacks[9–11]. Others highlight the roles of external forcing and model mean state: aerosol-forcing experiments suggest that fast atmospheric adjustment and ocean dynamical memory can help sustain early twenty-first-century La Niña-like conditions, and flux-adjusted simulations show that reducing tropical mean-state biases can produce a more La Niña-like response to radiative forcing[12,13]. Taken together, these studies show that Pacific SST trends are sensitive to circulation changes, remote ocean-atmosphere coupling, external forcing, and the simulated mean state.

They also suggest that mean-state and warming-pattern biases are connected. Yet they leave unresolved why free-running coarse-resolution models generate these linked biases in the first place.

One overlooked structural contributor may be the overly smoothed representation of the major mountain ranges of the Americas. The Rockies, Central American cordillera, and Andes form narrow, high barriers along the eastern Pacific margin, but coarse-resolution models represent these ranges with grid-cell mean elevations that underestimate crest heights and weaken mechanical blocking[14,15]. This height bias matters because these ranges define much of the eastern boundary of the Pacific. Previous studies show that American orography can influence cross-basin moisture transport, low-level winds, wind-driven ocean adjustment, subtropical subsidence, marine low clouds, eastern-boundary SSTs, and ITCZ structure[14–19]. Although these studies establish American orography as an important control on the Pacific mean state, they do not determine whether orographic smoothing can contribute directly to tropical Pacific rainfall biases through atmospheric moisture transport rather than coupled SST biases alone. Nor do they establish whether the resulting mean-state changes help explain errors in the simulated historical Pacific warming pattern.

Higher-resolution models can reduce some Pacific rainfall, SST, and warming-pattern biases, but resolution changes many processes at once, including topography, clouds, coastal winds, ocean dynamics, numerics, and parameterizations[20–23]. Existing topographic sensitivity experiments have clarified how individual mountain ranges affect regional circulation and eastern-Pacific climate, but most have not tested whether restoring the peak elevations of the Rockies, Central American cordillera, and Andes together can alter the coupled Pacific mean state and its historical warming pattern. In addition, broad maximum-height corrections can raise extensive terrain and introduce thermal forcing, making it difficult to isolate mechanical blocking effects[15,24]. A targeted perturbation is therefore needed to isolate the mechanical effects of restoring narrow American mountain peaks.

Here we test this hypothesis by selectively restoring more realistic peak elevations of the Rockies, Central American cordillera, and Andes while minimizing broad thermal forcing. Prescribed-SST experiments isolate the direct atmospheric response to higher topography, fully coupled simulations reveal the resulting ocean-atmosphere adjustment, and historical ensembles test whether the same perturbation affects the recent warming pattern. These experiments show that higher American mountains strengthen the mechanical barrier to low-level flow, reduce Atlantic/Amazon-to-Pacific moisture transport, and weaken the spurious southern tropical rain band. In coupled simulations, associated changes in eastern-Pacific subsidence, winds, upwelling, and marine low clouds reduce several Pacific SST mean-state biases. In historical simulations, the same topographic perturbation produces a more realistic northeastern Pacific warming pattern through enhanced low-cloud radiative cooling. These results identify smoothed American orography as a physically interpretable boundary-condition error linking Pacific mean-state biases to errors in simulated recent warming.

Results and Discussion

Direct atmospheric response: moisture transport and precipitation

To separate the immediate atmospheric effects of higher American topography from slower ocean-atmosphere feedbacks, we first analyze prescribed-SST simulations in which sea-surface temperatures are fixed and only the atmosphere responds to the orographic perturbation. We compare a Control simulation with default orography to a HITOPO simulation that raises the model crest grid cell at each latitude to the corresponding observed elevation. This design enhances the mechanical blocking of narrow mountain ranges while limiting broad thermal forcing (Methods; Supplementary Figure 1).

In the prescribed-SST experiments (Fig. 2), the Control simulation exhibits two prominent tropical precipitation biases even in the absence of SST errors. First, precipitation is excessive and the northern-hemisphere ITCZ is overly broad, a bias also present in the coupled configuration. Second, an unrealistically strong southern off-equatorial rain band develops over the central/eastern Pacific[25]. The persistence of these features under prescribed SSTs indicates that major components of the double-ITCZ structure are not solely a consequence of coupled SST biases, but have an atmospheric component, consistent with AMIP-based studies of double-ITCZ behavior[26].

Increasing American topography in HITOPO strengthens large-scale subsidence over the eastern subtropical and tropical Pacific and sharply reduces vertically integrated moisture transport across the tropical American transect (Fig. 2a,d). Tropical America is a known pathway for atmospheric freshwater export from the Atlantic/Amazon region toward the Pacific[16,17,27,28], and Central American mountains can obstruct Caribbean-to-eastern North Pacific moisture export[29]. In the Control simulation, net moisture transport toward the Pacific is 0.95 Sv, substantially larger than previous estimates for comparable cross-American transport: 0.36–0.47 Sv from Eulerian observation/reanalysis-based estimates and 0.26 Sv from a Lagrangian estimate[17,27,28,30]. In HITOPO, this transport decreases to 0.38 Sv, bringing the simulation into closer agreement with these estimates (Fig. 2d). The higher topography also enhances subsidence over the northeastern, southeastern, and eastern equatorial Pacific (Fig. 2a), providing an additional dynamical pathway for shifting tropical precipitation, consistent with previous work linking orographic subsidence to eastern Pacific rainfall structure[16,18].

Consistent with the reduced moisture import and enhanced eastern-Pacific subsidence, HITOPO produces a systematic shift in tropical precipitation (Fig. 2c). Precipitation decreases across the southern off-equatorial rain band (~5–15°S) over the central/eastern Pacific, with local drying up to ~3.6 mm day^{-1} in the prescribed-SST case. Rainfall also decreases along parts of the overly broad northern ITCZ, especially on its flanks, although the core ITCZ remains strong. Together, these changes weaken the characteristic double-ITCZ structure: the spurious southern branch is suppressed, while excessive northern-hemisphere rainfall is reduced in several biased regions.

Because SSTs are fixed, these precipitation shifts reflect a direct atmospheric response to altered orographic control of low-level flow, subsidence and inter-basin moisture pathways without air–sea coupling. The offshore precipitation improvement is accompanied by increased precipitation along parts of the American cordillera (Fig. 2c), likely reflecting enhanced local orographic uplift over steepened terrain and representing a caveat of the abrupt topographic perturbation.

Ocean-atmosphere response to higher topography

The prescribed-SST experiments isolate the direct atmospheric response to higher American topography: reduced cross-basin moisture transport, enhanced eastern-Pacific subsidence and weaker tropical precipitation biases. We next ask whether this pathway persists, weakens, or is reorganized when SSTs and ocean dynamics are allowed to respond. This step is essential because the historical warming pattern develops on a coupled mean state whose SST gradients, winds, upwelling, clouds, and precipitation interact with the response to external forcing. In the coupled configuration, the fixed-SST pathway partly persists: cross-basin moisture transport and eastern-Pacific precipitation bias are reduced, but these changes are now embedded within adjustments in SST gradients, low-level winds, upwelling, and marine clouds (Fig. 3; Supplementary Figure 2). This coupled step is important because double-ITCZ precipitation biases often coexist with persistent tropical Pacific SST mean-state errors, including an overly strong equatorial cold tongue[31–33].

Over the equatorial Pacific, HITOPO weakens the cold-tongue bias by warming the eastern equatorial Pacific and cooling the western Pacific, thereby reducing the zonal SST gradient (Fig. 3a). This mechanism differs from previous Central American-orography studies that emphasized surface heat-flux and ocean-current responses in shaping eastern tropical Pacific SSTs[15]. In HITOPO, eastern-equatorial warming is not driven by enhanced atmospheric heat input: net ocean heat uptake from the atmosphere decreases over this region (Supplementary Figure 3), indicating that surface heat-flux changes act mainly as a damping response. Instead, the warming is more consistent with ocean dynamical adjustment. HITOPO weakens low-level easterlies over the eastern equatorial Pacific while strengthening them farther west (Fig. 3a). These wind anomalies produce upper-ocean vertical-velocity changes that weaken upwelling in the east and strengthen it in the west (Fig. 3d). Reduced eastern-equatorial upwelling warms the equatorial surface and weakens the zonal SST gradient.

HITOPO also partially offsets the warm SST biases in the northeastern and southeastern subtropical Pacific, yielding pronounced coastal and subtropical cooling patches (Fig. 3a). These subtropical responses are consistent with previous work showing that American topography can strengthen subtropical anticyclonic circulation, descent, and marine low-cloud/SST feedbacks in the eastern Pacific[14,18,19]. In HITOPO, stronger northeasterly and southeasterly flow over the northeastern and southeastern Pacific favors cold advection and increased marine low-cloud cover, promoting regional SST cooling (Fig. 3a,c). Because eastern-boundary SST biases are also tied to coastal upwelling and marine low-cloud processes that are poorly resolved at coarse resolution, this topographic perturbation should be expected to alleviate only part of the bias[21,34].

These coupled SST and circulation changes feed back onto tropical precipitation. Rainfall increases modestly near the equator in the central/eastern Pacific, while cooling south of the equator suppresses convection and weakens the spurious southern off-equatorial rain band (Fig. 3b). Reduced cross-basin moisture transport also continues to limit moisture supply to the eastern Pacific (Supplementary Figure 2). The onshore precipitation increase along the American cordillera is weaker than in the prescribed-SST experiment, suggesting that coupled SST and circulation changes modify the upwind moisture supply and low-level flow impinging on the terrain. Overall, the coupled response is mechanistically connected to the prescribed-SST pathway but is not uniformly beneficial: allowing the ocean to adjust amplifies regional cooling and reorganizes SSTs, winds, clouds, and precipitation, reducing several Pacific biases while also suggesting possible over-adjustment to the imposed topography.

Historical warming pattern and cloud-stability mechanism

We next ask whether these orographically driven mean-state changes affect the simulated historical SST trend pattern. Applying the same modified orography in historical simulations improves several aspects of the 1979–2013 Pacific SST trend pattern: relative to the Control, HITOPO shows enhanced cooling over the northeastern Pacific, reduced warming rates over the southeastern and eastern equatorial Pacific, and enhanced warming over the western Pacific (Fig. 1c,d). Over the Pacific basin, HITOPO improves the centered pattern correlation with observations from -0.29 to 0.21 and reduces the area-weighted mean bias from 0.064 to 0.011 K decade^{-1}. These changes indicate that large-scale orography can substantially alter, and partly improve, the simulated historical warming pattern. We next examine whether the enhanced northeastern Pacific cooling arises through a pathway linking land-ocean thermal contrast, lower-tropospheric stability, marine low-cloud cover, and shortwave cloud cooling.

Low stratiform cloud cover over the subtropical northeastern Pacific off California peaks in boreal summer, when lower-tropospheric stability and inversion strength are strongest; this seasonality is associated with a strong negative shortwave cloud-radiative effect[35]. In HITOPO, the enhanced northeastern Pacific cooling trend is accompanied by a more negative shortwave cloud-radiative effect,

indicating reduced absorbed shortwave radiation at the surface (Fig. 4a), and by increased ECTEI over the same region, indicating stronger lower-tropospheric stability favorable for marine low clouds (Fig. 4b)[36,37].

These relationships are consistent with a warm-season land-ocean contrast mechanism acting on an orographically altered mean state. In JJA zonal-wind sections across western North America, higher topography raises the below-ground boundary from roughly 850–900 hPa in Control to near 700 hPa in HITOPO around 250°E, closing or strongly narrowing the low-level pathway across the mountain region (Supplementary Figure 4). This mean-state mechanical constraint helps explain why the topographic perturbation can affect the warming response: it changes the lower-tropospheric pathway through which the seasonally heated continent interacts with the northeastern Pacific marine boundary layer[38]. Monthly trend diagnostics then show the seasonal timing of this response: the land-ocean thermal contrast strengthens first, from late spring through October, while low-cloud and shortwave cloud-radiative responses peak later in summer (Supplementary Figure 5). Because these responses are strongest in boreal summer, we focus on JJA in the vertical sections.

The JJA sections show that the stronger land-ocean contrast trend in HITOPO is accompanied by enhanced stabilization below 800 hPa and increased low-cloud trends along 32.5°N (Fig. 4c,d). Together, these results support a mechanism in which higher orography alters the lower-tropospheric mean-state pathway across western North America, enhances warm-season land-ocean thermal contrast, strengthens northeastern Pacific boundary-layer stability, increases low-cloud cover, and amplifies shortwave cloud cooling and surface ocean cooling. More broadly, these results illustrate how an orographically altered mean state can affect the background on which historical warming patterns develop.

Synthesis and implications

Our results suggest that American mountain height influences not only the Pacific mean state, but also the simulated spatial pattern of historical warming. Together, the experiments identify mountain smoothing as a physically interpretable link between excessive cross-basin moisture transport, tropical precipitation biases, Pacific SST mean-state errors, and an unrealistic Pacific SST trend pattern. In prescribed-SST simulations, higher American topography reduces Atlantic/Amazon-to-Pacific moisture transport and enhances eastern-Pacific subsidence, weakening excessive tropical rainfall, especially the spurious southern rain band. When ocean-atmosphere coupling is allowed, the same perturbation reorganizes SST gradients, winds, clouds, and ocean dynamics. In historical simulations, this altered coupled background state produces a more realistic northeastern Pacific cooling trend through enhanced land-ocean thermal contrast, lower-tropospheric stability, low-cloud cover, and shortwave cloud cooling. These results imply that atmospheric responses to underestimated orographic forcing, together with their coupled ocean-atmosphere consequences, can contribute to biases in Pacific warming patterns and pattern-dependent climate feedbacks[7,8].

The response is not uniformly beneficial. The idealized topographic perturbation can introduce local precipitation artifacts, amplify regional cooling, and only partly alleviate biases where coarse model resolution still limits coastal upwelling and marine low-cloud processes. Because climate models are developed and tuned around their default orography, abrupt changes in mountain height may expose compensating errors or lead to overcorrection. Such overcorrection matters because Pacific SST gradients influence Walker circulation and El Niño-Southern Oscillation (ENSO) variability, while SST patterns shape radiative feedbacks; changes that improve individual regional biases could therefore still affect climate variability and feedback estimates[7,39,40]. These caveats suggest that topographic realism is not simply a matter of raising mountains, but of representing terrain-induced dynamical forcing in a physically based and numerically stable way.

The remaining mismatch over the southeastern Pacific points to processes beyond local American orography. Although HITOPO enhances shortwave cloud-radiative cooling there, it does not produce a cooling trend comparable to observations, suggesting that the southeastern Pacific trend is not controlled solely by local cloud feedbacks. Southern Ocean cooling may provide an additional influence through oceanic advection and large-scale atmospheric teleconnections[10,11], and a Southern Ocean pacemaker experiment combined with modified orography would provide a useful test of this interaction. The weaker southeastern response may also reflect a different seasonal low-cloud regime: unlike the northeastern Pacific, southeastern Pacific low-cloud cover peaks in austral spring and is much weaker in austral summer, when the land-ocean thermal contrast is largest[35].

More broadly, coastal topography along the Americas may help shape why the observed warming-cooling pattern is especially pronounced in the Pacific. By reinforcing subtropical anticyclonic circulation, stabilizing the marine boundary layer, and potentially amplifying the subtropical-cloud pathway linking Southern Ocean variability to the tropical Pacific[10,11,19], eastern Pacific coastal mountains may influence both regional SST trends and the feedbacks inferred from them. Improving the representation of topography may therefore strengthen confidence in projections of regional rainfall, SST trends, and associated climate feedbacks, but future work should pursue approaches that avoid the local artifacts and compensating-error risks introduced by abrupt topographic perturbations[24,41].

Methods

Observations

We obtained monthly sea surface temperature (SST) estimates from the Extended Reconstructed Sea Surface Temperature (ERSST) dataset on a 2° × 2° horizontal grid and calculated the linear trend for 1979–2013 shown in Fig. 1a. Monthly precipitation estimates were obtained from the Global Precipitation Climatology Project (GPCP) on a 2.5° × 2.5° horizontal grid. We averaged the years 1981–2010 to obtain the precipitation climatology shown in Fig. 2a. All observational datasets were regridded to the model resolution of 1.9° × 2.5° before analysis. We derived the topographic data used to construct the modified-orography experiment from the NOAA ETOPO 2022 Global Relief Model at 30-arcsecond resolution, as described below.

Model

We used the National Center for Atmospheric Research Community Earth System Model, version 1.2 (CESM1.2)[42], with the Community Atmosphere Model, version 5 (CAM5)[43]. The atmosphere was run with the finite-volume dynamical core at 1.9° × 2.5° horizontal resolution and 26 vertical layers. CESM1.2 provides a computationally tractable and well-documented framework for comparing atmosphere-only, coupled, and historical modified-orography experiments, while maintaining continuity with previous orographic sensitivity studies[14,19,44]. Its coarse horizontal resolution also makes it an appropriate testbed for this study because narrow mountain ranges are strongly smoothed and peak elevations are reduced.

As discussed in previous studies[14,15,19,24,44], the representation of orography in global climate models (GCMs) is a significant source of model biases, particularly in regions dominated by narrow mountain ranges such as the Andes, the Central American cordillera, and the Rocky Mountains. In coarse-resolution GCMs, topography is typically represented by the area-averaged observed elevation within each grid cell. This approach captures the broad thermal influence of mountains, which arises from elevation-dependent radiative effects, but it substantially oversmooths the terrain and underestimates peak elevations (Supplementary Figure 1). As a result, the mechanical effects of mountains are weakened, leading to biases in terrain-induced circulation, moisture transport and precipitation processes[29,45].

To better represent the mechanical influence of mountains on atmospheric flow, previous studies have replaced the grid-cell mean elevation with the maximum observed elevation within each grid cell (Supplementary Figure 1). Although this approach effectively enhances terrain-induced flow deflection, it can also exaggerate the thermal effect in broad plateau regions where the mean elevation is already reasonably represented. In such regions, the maximum-height method raises the surface too extensively and therefore introduces excessive thermal forcing[15].

To strengthen the mechanical influence of narrow mountain ranges while limiting broad thermal effects, we developed a refined strategy that is applied only to narrow mountain ranges, including the Rockies, Central American cordillera, and Andes (Supplementary Figure 1). Specifically, at each model latitude across the Americas, we identified the grid cell containing the maximum default model elevation and replaced that cell's elevation with the corresponding observed elevation from ETOPO 2022. As the observational baseline, we used the ETOPO 2022 dataset from the National Oceanic and Atmospheric Administration (NOAA) National Centers for Environmental Information, at 30-arcsecond resolution. Because the uplift is confined to the model grid cell corresponding to the existing mountain crest at each latitude, this method improves the representation of terrain-induced flow obstruction in narrow mountain ranges while minimizing changes to the large-area mean elevation. However, because some grid cells are still raised, the perturbation may retain localized thermal effects associated with elevation-dependent surface temperature and land-atmosphere energy exchange; we therefore interpret HITOPO as minimizing, rather than eliminating, thermal forcing.

We tested two topographic configurations in CESM: (1) a **Control** configuration using the default smoothed, area-averaged topography employed in coarse-resolution GCMs; and (2) a **HITOPO** configuration using the refined topography described above, in which the peak elevations of the Rockies, Central American cordillera, and Andes are selectively restored (Supplementary Figure 1). We performed simulations under prescribed-SST, fully coupled, and historical configurations to assess how the modified topography affects the simulated climatology in atmosphere-only and coupled settings, and how it influences the simulated pattern of historical climate change.

The AMIP-style simulations were integrated for 10 years under year-2000 climatological forcing, and the last 5 years were used for analysis. The fully coupled simulations were integrated for 500 years under preindustrial forcing, and the last 200 years were used to analyze the coupled response to the topographic modification. The equilibrated coupled simulations were then used to initialize historical ensembles. Historical simulations were run from 1979 to 2005 under historical forcing and extended from 2006 to 2013 under Representative Concentration Pathway 8.5 (RCP8.5) forcing, with nine ensemble members for both the Control and HITOPO configurations.

Moisture Transport

The cross-mountain moisture transport between 20°N and 20°S was calculated following a method similar to that of Richter and Xie[17]. We selected a comparable set of segments, illustrated in Fig. 2a, and defined the transport as

$$tr = \int_0^{ps} dP \int_0^L \frac{uqdl}{g}$$

where tr denotes the vertically integrated moisture transport across a given segment, $p$is atmospheric pressure, u is the wind component perpendicular to the segment line, defined as positive for flow from the Atlantic–Amazon region toward the Pacific, q is specific humidity, and g is gravitational acceleration. For each segment, the perpendicular moisture flux was integrated along the segment length and over the full atmospheric column from the surface to the top of the atmosphere.

Data availability

The Extended Reconstructed Sea Surface Temperature (ERSST) dataset is publicly available at https://www.ncei.noaa.gov/products/extended-reconstructed-sst. The Global Precipitation Climatology Project (GPCP) dataset is publicly available at https://www.ncei.noaa.gov/products/global-precipitation-climatology-project. The ETOPO 2022 dataset is publicly available at https://www.ncei.noaa.gov/products/etopo-global-relief-model. The Pacific Ocean mask is provided by the RECCAP2-ocean project and is available at https://github.com/RECCAP2-ocean/R2-shared-resources/blob/master/data/regions/RECCAP2_region_masks_all_v20221025.nc.

Figure-level processed data will be deposited in a public repository before publication; full monthly model output is available from the corresponding author upon reasonable request because of storage size.

Code availability

CESM1.2 is available from the National Center for Atmospheric Research at https://www.cesm.ucar.edu. The model configuration files, topography-processing scripts, and analysis and plotting scripts used in this study are available from the corresponding author upon reasonable request.

References

1. Zhang, S., Stier, P., Dagan, G., Zhou, C. & Wang, M. Sea surface warming patterns drive hydrological sensitivity uncertainties. *Nat. Clim. Chang.* **13**, 545–553 (2023).
2. Watanabe, M. *et al.* Possible shift in controls of the tropical Pacific surface warming pattern. *Nature* **630**, 315–324 (2024).
3. Wills, R. C. J., Dong, Y., Proistosecu, C., Armour, K. C. & Battisti, D. S. Systematic Climate Model Biases in the Large-Scale Patterns of Recent Sea-Surface Temperature and Sea-Level Pressure Change. *Geophysical Research Letters* **49**, e2022GL100011 (2022).
4. Seager, R., Henderson, N. & Cane, M. Persistent Discrepancies between Observed and Modeled Trends in the Tropical Pacific Ocean. *Journal of Climate* **35**, 4571–4584 (2022).
5. Kosaka, Y. & Xie, S.-P. Recent global-warming hiatus tied to equatorial Pacific surface cooling. *Nature* **501**, 403–407 (2013).
6. Dong, Y. *et al.* Biased Estimates of Equilibrium Climate Sensitivity and Transient Climate Response Derived From Historical CMIP6 Simulations. *Geophysical Research Letters* **48**, e2021GL095778 (2021).
7. Andrews, T. *et al.* On the Effect of Historical SST Patterns on Radiative Feedback. *Journal of Geophysical Research: Atmospheres* **127**, e2022JD036675 (2022).
8. Armour, K. C. *et al.* Sea-surface temperature pattern effects have slowed global warming and biased warming-based constraints on climate sensitivity. *Proceedings of the National Academy of Sciences* **121**, e2312093121 (2024).
9. England, M. H. *et al.* Recent intensification of wind-driven circulation in the Pacific and the ongoing warming hiatus. *Nature Clim Change* **4**, 222–227 (2014).
10. Dong, Y., Armour, K. C., Battisti, D. S. & Blanchard-Wrigglesworth, E. Two-Way Teleconnections between the Southern Ocean and the Tropical Pacific via a Dynamic Feedback. *Journal of Climate* **35**, 6267–6282 (2022).

11. Kim, H., Kang, S. M., Kay, J. E. & Xie, S.-P. Subtropical clouds key to Southern Ocean teleconnections to the tropical Pacific. *Proc. Natl. Acad. Sci. U.S.A.* **119**, e2200514119 (2022).

12. Hwang, Y.-T., Xie, S.-P., Chen, P.-J., Tseng, H.-Y. & Deser, C. Contribution of anthropogenic aerosols to persistent La Niña-like conditions in the early 21st century. *Proceedings of the National Academy of Sciences* **121**, e2315124121 (2024).

13. Zhuo, J.-Y. *et al.* A More La Niña–Like Response to Radiative Forcing after Flux Adjustment in CESM2. *Journal of Climate* **38**, 1037–1050 (2025).

14. Xu, W. & Lee, J.-E. The Andes and the Southeast Pacific Cold Tongue Simulation. *Journal of Climate* **34**, 415–425 (2021).

15. Baldwin, J. W., Atwood, A. R., Vecchi, G. A. & Battisti, D. S. Outsize Influence of Central American Orography on Global Climate. *AGU Advances* **2**, e2020AV000343 (2021).

16. Xu, H., Xie, S.-P., Wang, Y. & Small, R. J. Effects of Central American Mountains on the Eastern Pacific Winter ITCZ and Moisture Transport. *Journal of Climate* **18**, 3856–3873 (2005).

17. Richter, I. & Xie, S.-P. Moisture transport from the Atlantic to the Pacific basin and its response to North Atlantic cooling and global warming. *Clim Dyn* **35**, 551–566 (2010).

18. Takahashi, K. & Battisti, D. S. Processes Controlling the Mean Tropical Pacific Precipitation Pattern. Part I: The Andes and the Eastern Pacific ITCZ. *Journal of Climate* **20**, 3434–3451 (2007).

19. Chen, X., Lee, J.-E. & Wu, M. Seasonal Orographic Effect of North American Mountain Range at Different Levels and Its Remote Control on Tropical Climate. *Journal of Climate* **39**, 1841–1856 (2026).

20. Ma, J., Xu, S. & Wang, B. Warm bias of sea surface temperature in Eastern boundary current regions—a study of effects of horizontal resolution in CESM. *Ocean Dynamics* **69**, 939–954 (2019).

21. Moreno-Chamarro, E. *et al.* Impact of increased resolution on long-standing biases in HighResMIP-PRIMAVERA climate models. *Geoscientific Model Development* **15**, 269–289 (2022).

22. Dong, E. *et al.* The Process-Oriented Understanding on the Reduced Double-ITCZ Bias in the High-Resolution CESM1. *Geophysical Research Letters* **52**, e2024GL112087 (2025).

23. Kang, S. M. *et al.* Km-scale coupled simulation and model–observation SST trend discrepancy. *Proceedings of the National Academy of Sciences* **123**, e2522161123 (2026).

24. Meegan-Kumar, D. *et al.* Optimizing Topographic Boundary Conditions for East Pacific Climate Simulation. *Journal of Climate* **38**, 2497–2524 (2025).

25. Tian, B. & Dong, X. The Double-ITCZ Bias in CMIP3, CMIP5, and CMIP6 Models Based on Annual Mean Precipitation. *Geophysical Research Letters* **47**, e2020GL087232 (2020).

26. Xiang, B., Zhao, M., Held, I. M. & Golaz, J.-C. Predicting the severity of spurious "double ITCZ" problem in CMIP5 coupled models from AMIP simulations. *Geophysical Research Letters* **44**, 1520–1527 (2017).

27. Dey, D. & Döös, K. Atmospheric Freshwater Transport From the Atlantic to the Pacific Ocean: A Lagrangian Analysis. *Geophysical Research Letters* **47**, e2019GL086176 (2020).

28. Yang, J.-C., Zhang, Y., Richter, I. & Lin, X. Interannual Variability of Tropical Atlantic-to-Pacific Moisture Transport Linked to ENSO, Atlantic Niño, and the Freshwater Budget in the Northwestern Tropical Atlantic. *Journal of Climate* **34**, 4625–4641 (2021).

29. Fu, D. *et al.* Central American mountains inhibit eastern North Pacific seasonal tropical cyclone activity. *Nat Commun* **12**, 4422 (2021).

30. Zaucker, F. & Broecker, W. S. The influence of atmospheric moisture transport on the fresh water balance of the Atlantic drainage basin: General circulation model simulations and observations. *Journal of Geophysical Research: Atmospheres* **97**, 2765–2773 (1992).

31. Lin, J.-L. The Double-ITCZ Problem in IPCC AR4 Coupled GCMs: Ocean–Atmosphere Feedback Analysis. *Journal of Climate* **20**, 4497–4525 (2007).

32. Samanta, D., Karnauskas, K. B. & Goodkin, N. F. Tropical Pacific SST and ITCZ Biases in Climate Models: Double Trouble for Future Rainfall Projections? *Geophysical Research Letters* **46**, 2242–2252 (2019).

33. Zhang, Q., Liu, B., Li, S. & Zhou, T. Understanding Models' Global Sea Surface Temperature Bias in Mean State: From CMIP5 to CMIP6. *Geophysical Research Letters* **50**, e2022GL100888 (2023).

34. Richter, I. Climate model biases in the eastern tropical oceans: causes, impacts and ways forward. *WIREs Climate Change* **6**, 345–358 (2015).

35. Klein, S. A. & Hartmann, D. L. The Seasonal Cycle of Low Stratiform Clouds. *Journal of Climate* **6**, 1587–1606 (1993).

36. Wood, R. & Bretherton, C. S. On the Relationship between Stratiform Low Cloud Cover and Lower-Tropospheric Stability. *Journal of Climate* **19**, 6425–6432 (2006).

37. Kawai, H., Koshiro, T. & Webb, M. J. Interpretation of Factors Controlling Low Cloud Cover and Low Cloud Feedback Using a Unified Predictive Index. *Journal of Climate* **30**, 9119–9131 (2017).

38. Kloesel, K. A. Marine Stratocumulus Cloud Clearing Episodes Observed during FIRE. *Monthly Weather Review* **120**, 565–578 (1992).

39. Lee, S. *et al.* On the future zonal contrasts of equatorial Pacific climate: Perspectives from Observations, Simulations, and Theories. *npj Clim Atmos Sci* **5**, 82 (2022).

40. Cai, W. *et al.* Changing El Niño–Southern Oscillation in a warming climate. *Nat Rev Earth Environ* **2**, 628–644 (2021).

41. Adcroft, A. Representation of topography by porous barriers and objective interpolation of topographic data. *Ocean Modelling* **67**, 13–27 (2013).

42. Hurrell, J. W. *et al.* The Community Earth System Model: A Framework for Collaborative Research. *Bulletin of the American Meteorological Society* **94**, 1339–1360 (2013).

43. Neale, R. B. *et al. Description of the NCAR Community Atmosphere Model (CAM 5.0)*. https://www.cesm.ucar.edu/models/cesm1.0/cam/docs/description/cam5_desc.pdf (2012).

44. Xu, W., Lee, J.-E., Fox-Kemper, B., Planton, Y. & McPhaden, M. J. The Andes Affect ENSO Statistics. *Journal of Climate* **35**, 7077–7091 (2022).

45. Cannon, F. *et al.* Effects of topographic smoothing on the simulation of winter precipitation in High Mountain Asia. *Journal of Geophysical Research: Atmospheres* **122**, 1456–1474 (2017).

Acknowledgements

This work was supported by the U.S. National Science Foundation (NSF) under Grant EAR-2103011.We acknowledge high-performance computing support from OSCAR, provided by the Center for Computation and Visualization at Brown University. We thank Baylor Fox-Kemper and Jared M. Kodero for constructive comments that improved the manuscript, and Paul Hall for assistance with model simulations. We also thank Wenhao Zhao and Hairuo Fu, researchers in other fields, for suggestions that helped keep the manuscript broadly readable.

Author contributions

X.C. and J.-E.L. conceived the study and designed the model experiments. X.C. performed the simulations, analyzed the data, prepared the figures, and wrote the initial manuscript draft. X.C. and J.-E.L. interpreted the results and revised the manuscript.

Competing interests

The authors declare no competing interests.

Figures

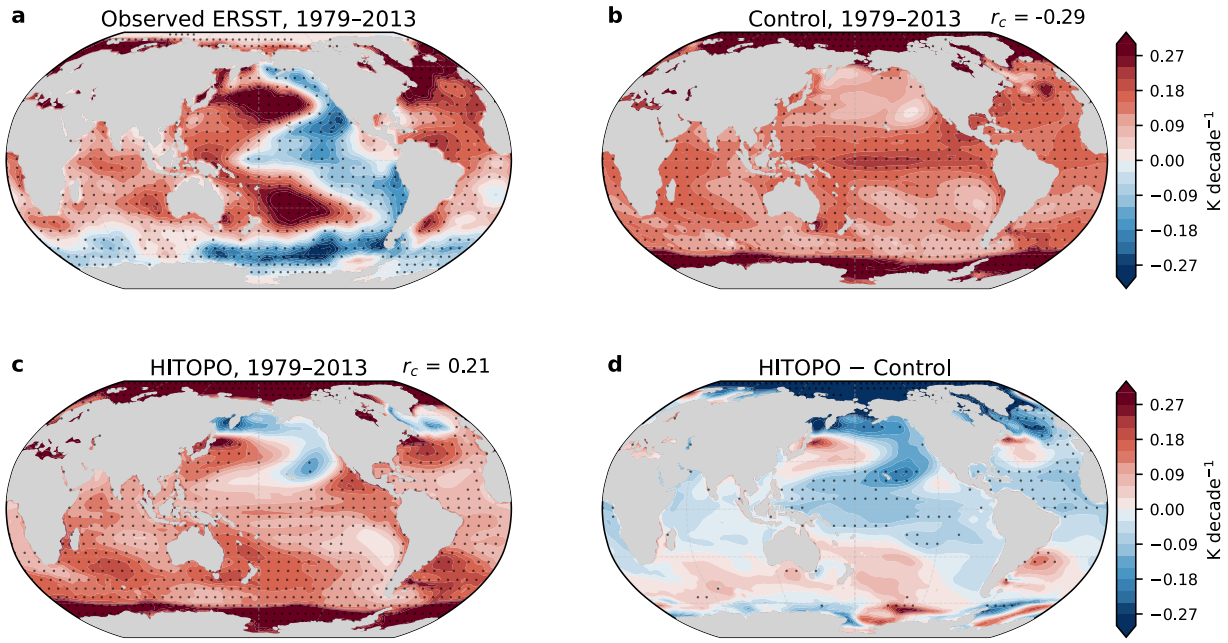

Figure 1. Observed and simulated SST trends over 1979–2013. Observations show **a** pronounced zonal asymmetry in Pacific SST trends, whereas the Control simulation exhibits broadly uniform warming with little cooling. HITOPO produces a stronger cooling response, particularly over the northeastern Pacific (NEP). **a**, Observed ERSST SST trend. **b**, Control SST trend. **c**, HITOPO SST trend. **d**, Difference in SST trend between HITOPO and Control (HITOPO − Control). Stippling indicates regions where the trends or trend differences are statistically significant. Numbers in **b** and **c** denote the centered pattern correlation (r_c) relative to observed ERSST trends, computed over the Pacific basin using RECCAP ocean mask.

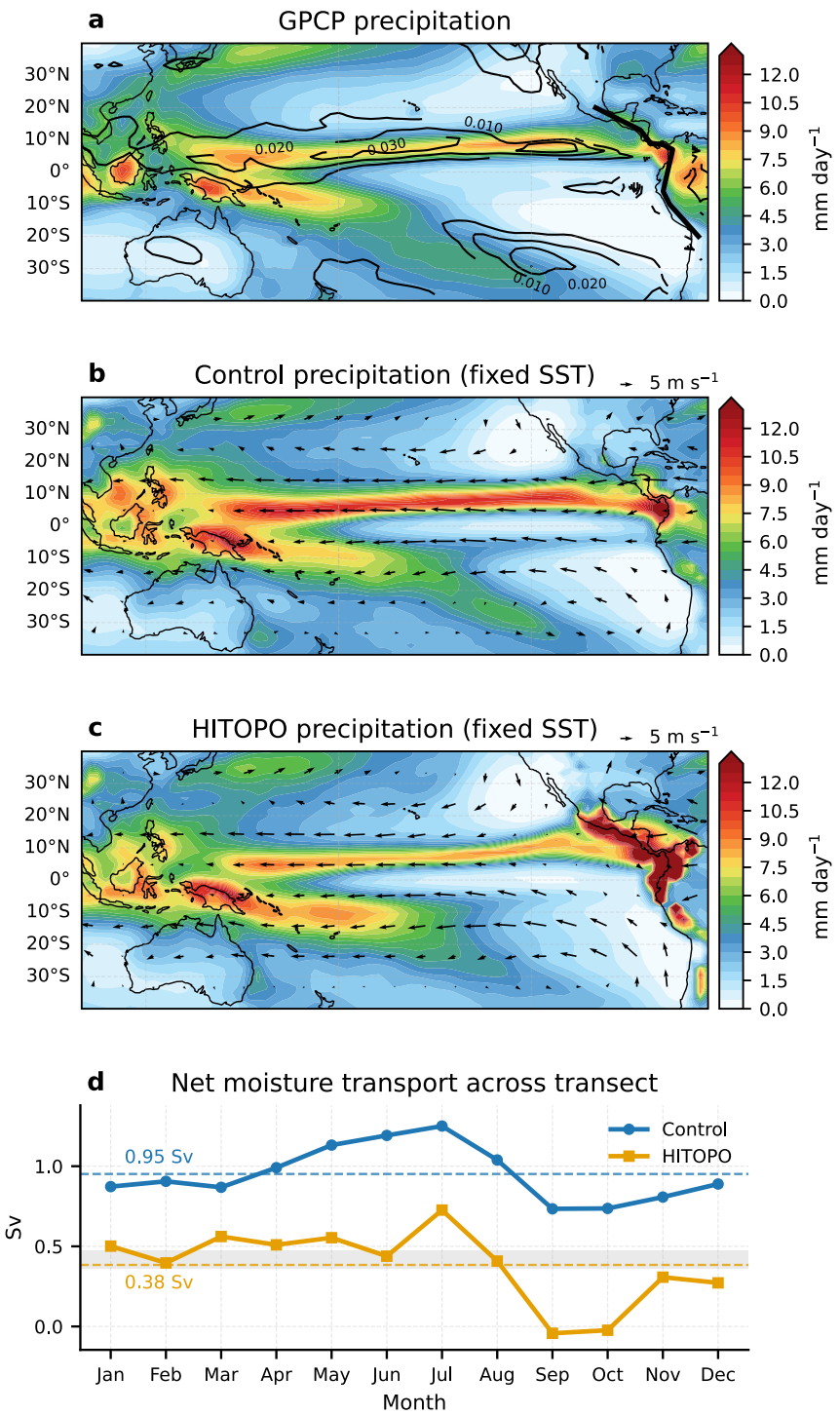

Figure 2. Mean precipitation, low-level winds, and cross-mountain moisture transport in prescribed-SST experiments. The Control simulation exhibits excessive precipitation and a pronounced double-ITCZ bias, whereas HITOPO reduces these biases, consistent with weaker zonal moisture transport into the eastern Pacific. **a**, Observed precipitation from the Global Precipitation Climatology Project (GPCP) for 1981–2010; contours show the annual-mean change in 500-hPa pressure velocity ($\Delta\omega_{500}$; Pa s^{-1}; HITOPO − Control), with positive values indicating enhanced subsidence. The black line

marks the transect used in **d**. **b**, Control simulation. **c**, HITOPO simulation. Shading in **a**–**c** shows annual-mean total precipitation rate (mm day^{-1}); black vectors in b,c indicate 850-hPa horizontal winds (reference vector, 5 m s^{-1}). **d**, Monthly vertically integrated moisture transport across the transect shown in a for the Control and HITOPO simulations (Methods); positive values indicate transport toward the Pacific. Horizontal dashed lines denote the annual-mean transport in each simulation, and the grey band indicates observational Eulerian estimates (0.36–0.47 Sv).

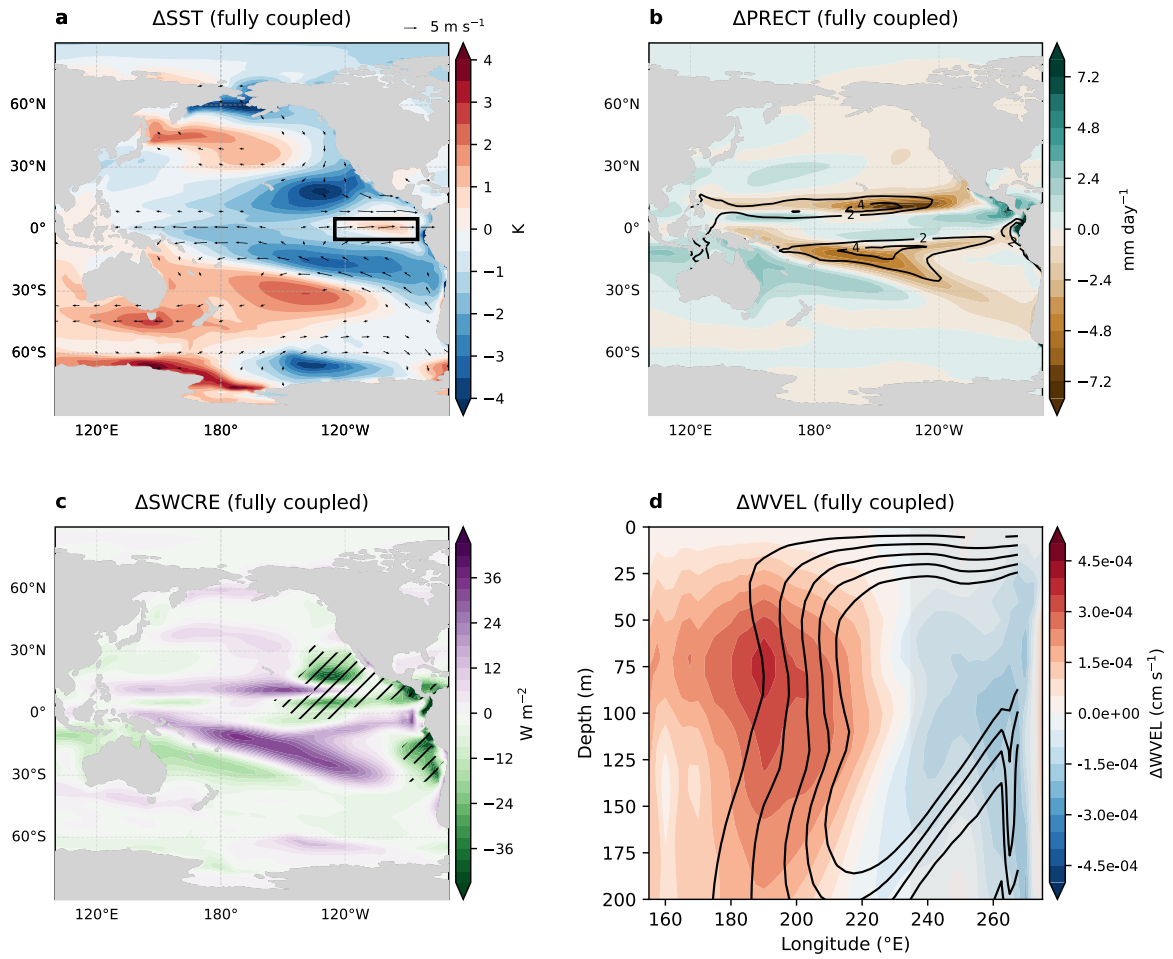

Figure 3. Annual-mean coupled response in HITOPO relative to Control. HITOPO reduces the eastern Pacific cold-tongue bias, accompanied by weaker low-level winds over the eastern equatorial Pacific and a reduced upwelling response. **a,** Sea surface temperature change (ΔSST; HITOPO − Control, K), with 850-hPa wind anomalies shown as vectors. **b,** Change in annual-mean total precipitation rate (ΔPRECT; mm day^{-1}; HITOPO − Control); contours indicate the precipitation bias in the Control simulation relative to GPCP observations for 1981–2010. **c,** Change in shortwave cloud radiative effect (ΔSWCRE; W m^{-2}); hatching marks regions where low-cloud fraction increases over the eastern tropical and subtropical Pacific. **d,** Change in vertical velocity (ΔWVEL; HITOPO − Control) in the equatorial Pacific sector, averaged over 5°S–5°N and shown for the upper 200 m. Contours denote the Control climatology of mean upwelling. The gray band marks the longitudinal extent of the black box in **a**, highlighting the surface-warming region.

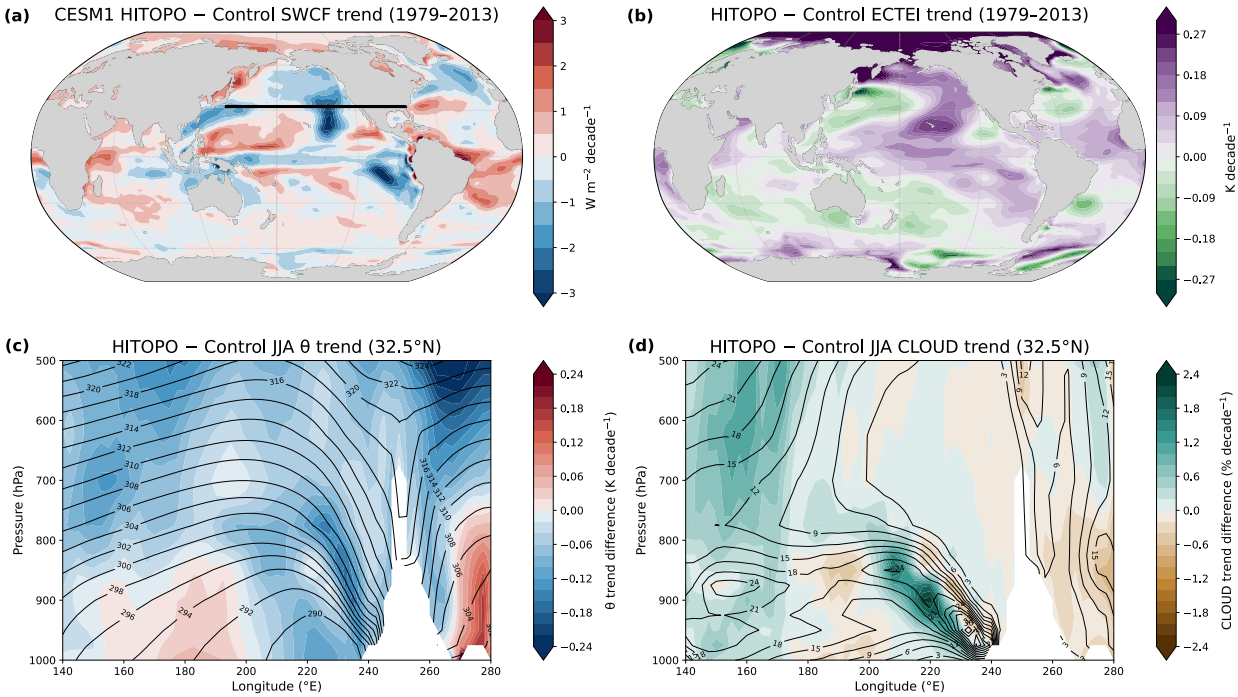

Figure 4. Mechanism for the enhanced cooling trend over the northeastern Pacific. Enhanced cooling over the northeastern Pacific is associated with a strengthened shortwave cloud radiative effect, which reduces incoming shortwave radiation. This enhanced cloud effect is linked to a stronger increase in lower-tropospheric stability, particularly in summer, driven by an enhanced land–ocean thermal contrast and accompanied by increased low-level cloud. **a,** SWCF trend difference (HITOPO − Control) for 1979–2013. **b,** Estimated Cloud-Top Entrainment Index (ECTEI) trend difference (HITOPO − Control) for 1979–2013. **c,** JJA potential temperature trend difference along 32.5°N (shading), with Control climatology shown by contours. **d,** JJA cloud trend difference along 32.5°N (shading), with Control climatology shown by contours. Panels **c,d** are vertical sections averaged over 32.5°N ± 1° along the black line in **a**.

Supplementary Files

This is a list of supplementary files associated with this preprint. Click to download.

- SupplementaryInformationCEE.pdf